Automatic detection of ischemic stroke using higher order spectra features in brain MRI images

Dear author,

Please note that changes made in the online proofing system will be added to the article before publication but are not reflected in this PDF.

We also ask that this file not be used for submitting corrections.

COGSYS 859
30 May 2019
ARTICLE IN PRESS
No. of Pages 9, Model 5+

Available online at www.sciencedirect.com
ScienceDirect
Cognitive Systems Research xxx (xxxx) xxx
Cognitive Systems RESEARCH
www.elsevier.com/locate/cogsys

Automatic detection of ischemic stroke using higher order spectra features in brain MRI images

U. Rajendra Acharya [a,b,c,*], Kristen M. Meiburger [d], Oliver Faust [e], Joel En Wei Koh [a], Shu Lih Oh [a], Edward J. Ciaccio [f], Asit Subudhi [g], V. Jahmunah [a], Sukanta Sabut [h]

[a] Department of Electronics and Computer Engineering, Ngee Ann Polytechnic, Singapore
[b] Department of Biomedical Engineering, School of Science and Technology, Singapore University of Social Sciences, Singapore
[c] School of Medicine, Faculty of Health and Medical Sciences, Taylor's University, Subang Jaya, Malaysia
[d] Department of Electronics and Telecommunications, Politecnico di Torino, Italy
[e] Department of Engineering and Mathematics, Sheffield Hallam University, United Kingdom
[f] Department of Medicine, Columbia University, College of Physicians and Surgeons, NY, USA
[g] Dept. of ECE, ITER, SOA Deemed to be University, Odisha, India
[h] School of Electronics Engineering, KIIT Deemed to be University, Odisha, India

Received 18 February 2019; received in revised form 29 April 2019; accepted 10 May 2019

Abstract

The gravity of ischemic strokes is the key factor in deciding upon the optimum therapeutic intervention. Ischemic strokes can be divided into three main groups: lacunar syndrome (LACS), partial anterior circulation syndrome (PACS), and total anterior circulation stroke (TACS), where the corresponding severity is mild, medium, and high, respectively. Herein, a unique method for the automatic detection of ischemic stroke severity is presented. The proposed system is based upon the extraction of higher order bispectrum entropy and its phase features from brain MRI (Magnetic Resonance Imaging) images. For classification, which is used to establish stroke severity, a support vector machine was incorporated into the design. The developed technique effectively detected the stroke lesion, and achieved a sensitivity, specificity, accuracy, and positive predictive value equal to 96.4%, 100%, 97.6% and 100%, respectively. The results were obtained without the need for manual intervention. This design is advantageous over state-of-the-art automated stroke severity detection systems, which require the reading neuroradiologist to manually determine the region of interest. Hence, the method is efficacious for delivering decision support in the diagnosis of ischemic stroke severity, thereby aiding the neuroradiologist in routine screening procedures.

Keywords: Ischemic stroke; Entropy; Bispectrum; Classifier; ADASYN; HOS

1. Introduction

Ischemic stroke results from a lack of blood supply to a specific region of the brain (Fig. 1). This diminishes the basic functions of nerve cells in the affected brain area, and can lead to significant long-term disability. Stroke is

* Corresponding author at: Department of Electronics and Computer Engineering, Ngee Ann Polytechnic, Singapore 599489, Singapore.
E-mail address: aru@np.edu.sg (U. Rajendra Acharya).

https://doi.org/10.1016/j.cogsys.2019.05.005
1389-0417/

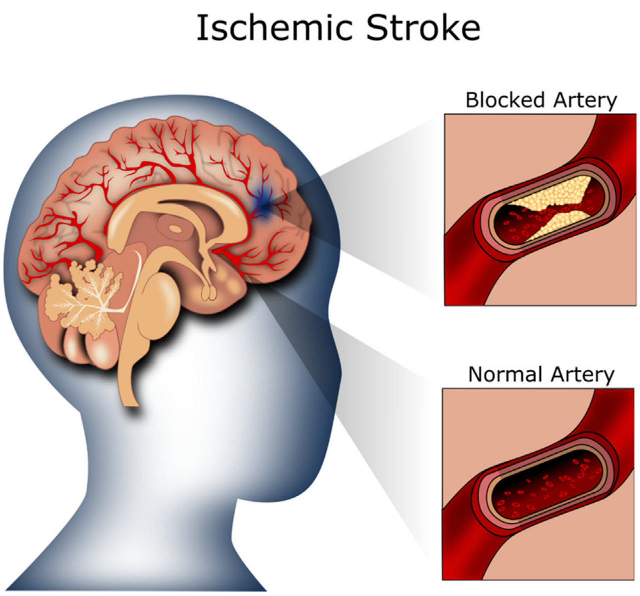

Fig. 1. Illustration of ischemic stroke.

a worldwide issue, being the second leading cause of death and the third leading cause of disability (Bonita, 1992). Ischemic strokes can be grouped into one of *three* types (Lindgren, Norrving, Rudling, & Johansson, 1994):

1. Partial anterior circulation syndrome (PACS): the middle/anterior cerebral regions are affected due to this type of stroke.
2. Lacunar syndrome (LACS): this stroke results from the occlusion of vessels that provide blood to the deep brain regions;
3. Total anterior circulation stroke (TACS): middle/anterior cerebral regions are affected due to a massive brain stroke.

Osmani, Durrani, and Ara (2010) compared the outcome in these three different types of stroke. A chi-squared test was employed to compare proportion difference in results across the different types strokes, with $p < 0.05$ considered to be statistically significant. They established that TACS has the worst outcome with the highest number of mortalities, whereas LACS had a better outcome. To be specific, a majority of LACS patients were functionally independent after 6 months. The patients with PACS had an average outcome, better than those with TACS, but not as positive as those with LACS.

In order to decide upon therapeutic intervention, the diagnosis, along with the severity of the ischemic stroke, are of fundamental importance (Zaidi, 2012). MRI images contain salient information for classification of ischemic stroke severity. However, the scan results are difficult to analyze, because subtle changes in the images are the points that are indicative of stroke severity. This difficulty translates into a long time spent in manual image analysis. Executing the mental tasks necessary to establish stroke severity causes fatigue, and in turn fatigue may lead to human error, which lowers diagnostic quality. Apart from fatigue, inter- and intra-observer variability exists for all human-based classification methodology. Education of the clinical analyst is a tool that can partially ameliorate these pitfalls. Yet, training a person to the expert level is time consuming and expensive, which makes routine stroke risk estimation tasks uneconomical.

Scientists and engineers have addressed these problems by developing reliable methods for the automatic detection of ischemic stroke severity. Recent research focuses on design systems which aid reading neuroradiologists by reducing both the amount and duration of routine tasks. Numerous studies in the literature focus on the diagnosis of ischemic stroke in magnetic resonance imaging (MRI) of the brain. Among the various MRI imaging modalities, diffusion weighted imaging (DWI) is quite sensitive to small water diffusion changes in the acute ischemic brain, and is therefore often used for timely stroke detection (Lutsep et al., 1997; Newcombe, Das, & Cross, 2013). Many previous ischemic stroke classification methods were based upon an intimal segmentation of the brain lesion within the image, ranging from the use of simple edge-based and threshold-based methods (Carson, Belongie, Greenspan, & Malik, 2002; Wang, Xiang, Pan, Wang, & Meng, 2013) to clustering-based and supervised methods (Ji, Xia, & Zheng, 2017; Sridevi & Mala, 2019) to methods based on Delaunay triangulation (Subudhia, Dash, Jena, & Sabut, 2018). The downside to these techniques is that, since the segmentation is the first stage of the entire classification process, an inaccurate segmentation of the brain lesion, within the DWI image, percolates throughout the processing chain. As a result, even small variations during image segmentation have a disproportionally large effect on ischemic stroke classification. Prior studies have supposed perfect image segmentation, which is difficult to achieve in practice. Thus, the possibility of an imperfect image segmentation is expected to have a negative impact on ischemic stroke classification quality in a practical setting.

Artificial intelligence techniques have been used in medical applications to predict diseases and the outcome in ischemic stroke patients (Scalzoa et al., 2013). Ramli, Ghazali, and Tay (2018) employed three emboli detection techniques; the sinusoidal model, energy and zero crossing rate and short time average zero crossing rate to examine the spectrum of high magnitude frequency element. Sinusoidal modelling yielded the highest accuracy of 84.2% for the classification of ischemic stroke. Chin, Lin, Wu, Weng, Yang, and Su (2017) developed a network using deep learning algorithms, to classify ischemic stroke automatically and obtained an accuracy of more than 90%. Many other methods have also been deployed using

Please cite this article as: U. Rajendra Acharya, K. M. Meiburger, O. Faust et al., Automatic detection of ischemic stroke using higher order spectra features in brain MRI images , Cognitive Systems Research, https://doi.org/10.1016/j.cogsys.2019.05.005

machine learning to confront issues of lesion segmentation and/or classification (Feng, Zhao, & Huang, 2016; Hemanth, Vijila, Selvakumar, & Anitha, 2013; Hevia-Montiel, 2007; Mitra, 2014), and yet, the majority of techniques still depend strongly upon a first accurate segmentation of the lesion.

Recently, higher order spectra (HOS) methods have been effectively used to pick the minute details in the signals and images (Martis, Acharya, Mandana, Ray, & Chakraborty, 2013; Noronha, Acharya, Nayak, Martis, & Bhandary, 2014; Swapna, Rajendra Acharya, Vinithasree, & Suri, 2013). The bispectrum entropy and phase features have been effectively used in many applications, such as in cardiac decisions (Martis et al., 2013), the diagnosis of fatty liver disease and cirrhosis (Acharya et al., 2015; Acharya, 2016), and in thyroid nodule severity diagnosis (Raghavendra, 2018).

In this study, we aim to provide an automatic detection of ischemic stroke severity using machine learning techniques, without employing any segmentation method that relies upon the calculation of higher-order bispectrum entropy features on the input DWI image, overcoming the problems that can derive from inaccurate lesion segmentation.

2. Materials and methods

This section introduces the materials and methods used to develop the proposed stroke severity classification system. The basic idea behind the system design is to find discriminative features which extract diagnostically relevant information from DWI images. Feature extraction is necessary, because the machine learning algorithms, in our case the SVM, cannot readily address high dimensional data, such as is typically found in biomedical imagery. The feature extraction projects the image into a lower dimensional space, which is then input to a machine classifier. Fig. 2 provides an overview block diagram of the system. The subsequent sections introduce the functionality of the individual blocks.

2.1. Image database

The dataset used in this study was obtained from stroke patients at the IMS and SUM Hospital, Bhubaneswar, Odisha, India, and each patient had a prominent visible stroke lesion evident within the image. All images were acquired with Signa HDxT 1.5 T Optima Edition (GE Healthcare, Waukesha, WI) and were exported for offline processing. The ethics committee approved the study, and the patients signed an informed consent before to being included. The image database consisted of 267 brain MRI images using the DWI modality, including 3 different stroke types. There were 18 images relative to LACS, 222 images relative to PACS, and 27 images relative to TACS. Fig. 3 shows an example image for each stroke type.

Table 1 summarizes the image data details. Column 2 of Table 1 details the number of images in the original dataset. There are only 18 LACS images, which is a small series compared to the 222 PACS images. Hence, the initial database is imbalanced. To address this problem, we used a synthetic sample method to balance the three considered classes. Column 3 indicates the amount of synthetic data generated for the individual classes. Column 4 states the total number of images, i.e. the sum of original and synthetic images. The process of generating synthetic images is described in Sections 2.2–4.

2.1.1. ADASYN synthetic sampling

In classification and learning methods, it is of fundamental importance to have a balanced dataset in order to avoid biasness due to disproportionate data distribution. Adaptive synthetic sampling (ADASYN) is employed to boost the performance, by decreasing the bias and balancing the samples (Haibo, Yang, Garcia, & Shutao, 2008; Molinari, Raghavendra, Gudigar, Meiburger, & Rajendra Acharya, 2018). It is apparent in part 2.1, the initial database is very imbalanced, with a high bias toward images with PACS. To overcome this issue, we employed ADASYN to balance the database. ADASYN first evaluates the disproportion among different classes, and produces the number of synthetic data for the minority classes thereafter, according to the density distribution. The quantity of synthetic samples to be simulated are evaluated by the following equation: $(m_1 - m_S) \times \beta$, where β is an empirical parameter between 0 and 1. In this study, we chose $\beta = 1$ to obtain the optimal performance. After ADASYN employment, the database then consisted of 223 LACS images, 222 PACS images, and 222 TACS images (Table 1), for a total of 667 images.

2.2. Automatic stroke detection approach

2.2.1. Image preprocessing and Radon transform

During the initial processing step, each image underwent adaptive histogram equalization (Pizer, 1987) in order to enhance the image and increase contrast. The histogram equalization algorithm used local regions within which the contrast is amplified in an adaptive manner.

After equalization, the images were processed with the Radon transform (RT). This projects the pixel values along a radial line at a particular angle onto a two dimensional

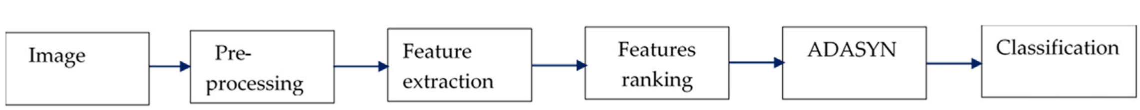

Fig. 2. Flowchart of the proposed system.

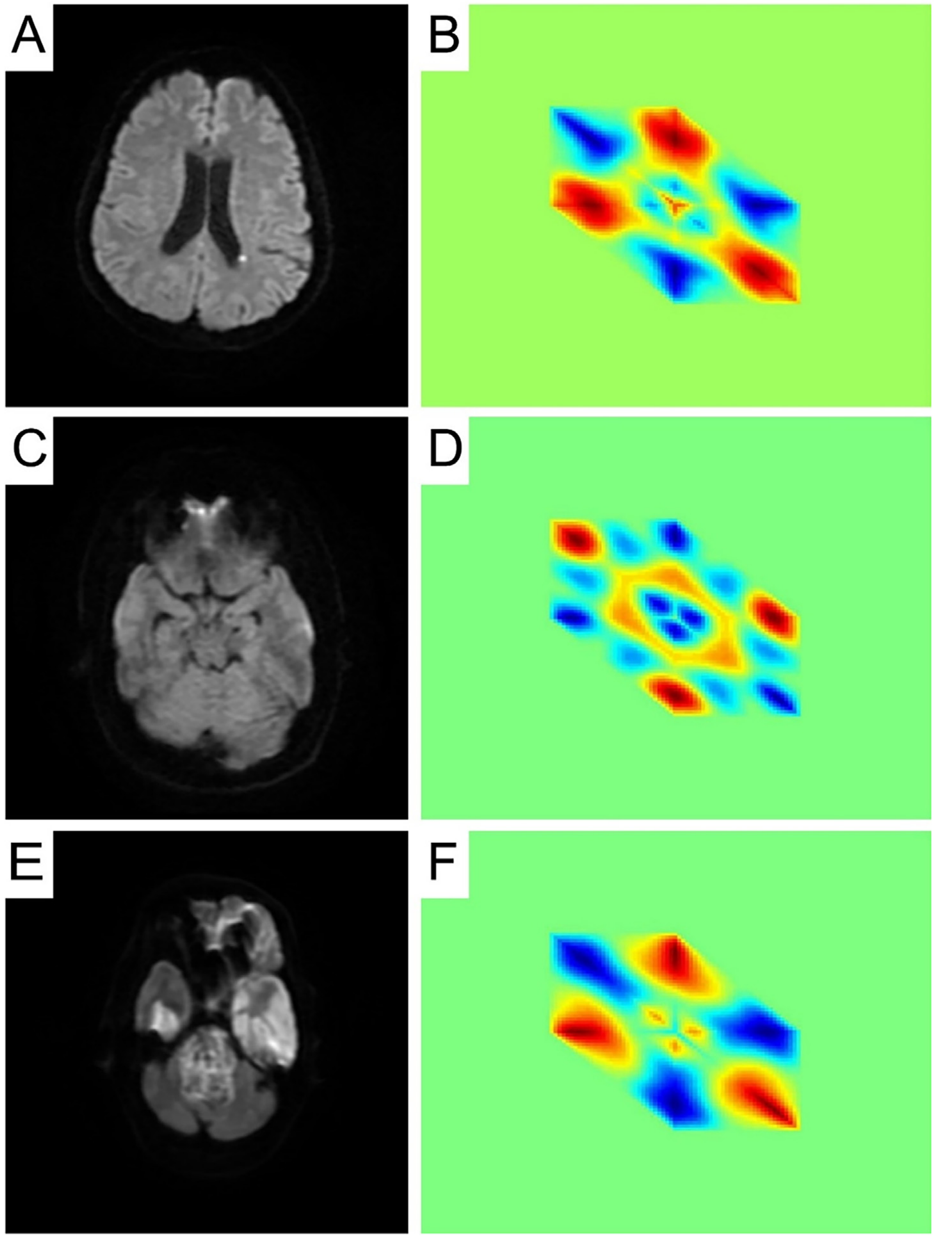

Fig. 3. Examples of ischemic strokes and bispectrum images. (A) MRI image of LACS stroke (B) bispectrum image of LACS stroke (C) MRI image of PACS stroke (D) bispectrum image of PACS stroke (E) MRI image of TACS stroke (F) bispectrum image of TACS stroke.

Table 1
Summary of number of data.

Class	Actual	Synthetic	Gross
LACS	18	205	223
PACS	222	0	222
TACS	27	195	222

graph. Algorithmically, the mathematical operation is modeled as a summing the values of pixel in the observed direction (Radon, 1986). The RT is therefore capable of capturing specific directional signatures from an image, and simultaneously preserving intensity distinctions, to enhance image spatiofrequency information. In this study, we calculated the RT from 0° to 179°, with a step size of 1°.

2.2.2. Feature extraction

In this step, we extracted features based on Higher Order Spectra (HOS) and various entropies.

2.2.2.1. Higher order spectra (HOS). Using the obtained 180 1D RT sinogram signals were extracted the higher-order bispectrum entropy and phase features (Nikias & Raghuveer, 1987). The bispectrum plots are shown in Fig. 3B, D, F for LACS, PACS and TACS types of stroke respectively.

Please cite this article as: U. Rajendra Acharya, K. M. Meiburger, O. Faust et al., Automatic detection of ischemic stroke using higher order spectra features in brain MRI images , Cognitive Systems Research, https://doi.org/10.1016/j.cogsys.2019.05.005

Various bispectrum entropies (first, second, third order entropies and phase entropies) were extracted as presented in (Chua, Chandran, Acharya, & Lim, 2008; Chua, Chandran, Acharya, & Lim, 2008). The bispectrum therefore is a non-linear method for analyzing images and is able to detect subtle image variation.

2.2.2.2. Entropy features. Entropy is a measure of uncertainty, which is associated with the randomness of the measured structure. In this study, we used seven different measurements of entropy, which are defined here and are explained in more detail in Singh and Singh (2010):

Given that an image $I(x,y)$ has N_i distinct gray levels (where $i = 0, 1, \cdots, L_{i-1}$), the normalized histogram from a specific region-of-interest (ROI) with dimensions $(A \times B)$ can be defined as:

$$F_i = \frac{N_i}{A \times B} \tag{2}$$

Therefore, Shannon entropy can be expressed as:

$$S_n = -\sum_{i=0}^{L-1} F_i \log_2 F_i \tag{3}$$

Yager entropy can be expressed as:

$$Y = \frac{\sum_{i=0}^{L-1} |2F_i - 1|}{|A \times B|} \tag{4}$$

Kapur entropy can be expressed as:

$$K_{\alpha,\beta} = \frac{1}{\beta - \alpha} \log_2 \frac{\sum_{i=0}^{L-1} F_i^{\alpha}}{\sum_{i=0}^{L-1} F_i^{\beta}} \tag{5}$$

where $\alpha \neq \beta, \alpha > 0, \beta > 0$.

Rényi entropy can be expressed as:

$$R = \frac{1}{1-\alpha} \log_2 \sum_{i=0}^{L-1} F_i^{\alpha} \tag{6}$$

Vajda entropy is a special case of the Kapur entropy where $\beta = 1$, and can be defined as:

$$V_{\alpha} = \frac{1}{1-\alpha} \log_2 \frac{\sum_{i=0}^{L-1} F_i^{\alpha}}{\sum_{i=0}^{L-1} F_i} \tag{7}$$

Fuzzy entropy can be expressed as:

$$S_n = -\sum_{i=0}^{L-1} F_i \log_2 F_i \tag{8}$$

Max entropy can be expressed as:

$$S_n = -\sum_{i=0}^{L-1} F_i \log_2 F_i \tag{9}$$

2.2.3. Feature ranking

Feature ranking and the subsequent feature selection plays an important role when building a robust learning model, because these steps will determine which information is presented to the machine classification system. There are various statistical techniques that can be used for selecting significant features. A particular feature can be considered more important if we can rank the feature among the other features based on some metric. Therefore, a higher ranked feature is more valuable for classification than a lower-ranked feature. Moreover, ignoring features that have a rank lower than a specific threshold can also increase classification speed.

In this study, the computed features were ranked using the F-value obtained from analysis of variance (ANOVA) (Hoaglin & Welsch, 1978). The features with higher F-values are ranked first, and vice-versa. We input the highest ranked features first to the classifiers in the descending order one by one in the descending order until the highest performance is achieved.

2.2.4. Classification and validation

The following classification methods were utilized in our three-class system: decision tree (DT), linear discriminant analysis (LDA), quadratic discriminant analysis (QDA), k-nearest neighbor (k-NN), probabilistic neural network (PNN), and support vector machine (SVM) with ten-fold strategy. The SVM classifier (polynomials 1 to 3) and radial basis function (RBF) kernels were used (Duda, Hart, & Stork, 2012). Acharya et al. (2016) provides a detailed description of each of these classification methods.

As discussed in the Introduction, LACS is considered a mild stroke, whereas PACS and TACS are considered as medium and severe strokes, respectively. Therefore, for the calculation of the validation parameters, a LACS is considered as a negative, whereas PACS and TACS are considered as a positive. Hence, the number of true negatives correspond to the number of LACS images correctly classified as LACS images, whereas the number of true positives correspond to the number of PACS and TACS images that are correctly classified.

3. Results

The completely automatic approach presented herein relies first upon image preprocessing, and then on the extraction of specific features, specifically image entropies and higher order spectra entropy and phase features. The final number of features for each image was equal to 79. These features were ranked according to the ANOVA F-value, and the top 45 ranked features are reported in Table 2. Fig. 4 provides a graphical representation of the feature performance based upon the F-value. As can be observed, the higher order bispectrum entropy and phase features are the highest ranked features, and are therefore the most discriminant for the determination of ischemic stroke with brain MRI imagery.

The final results of classification and the number of features used for each method are reported in Table 3. As can be noted, the SVM with RBF kernel provided the best results, using a total number of 36 features (i.e., the first

Table 2
Top 45 features sorted using the ANOVA (F-value).

Feature	LACS		PACS		TACS			
	Mean	SD	Mean	SD	Mean	SD	p-value	F-value
HOS Ent_1^{17}	0.5655	0.1848	0.4761	0.1635	0.3224	0.1902	0.0000	13.4663
HOS Ent_2^{18}	0.4976	0.2091	0.3895	0.2301	0.1918	0.1344	0.0000	12.4899
HOS Ent_1^{18}	0.6514	0.0944	0.5516	0.1731	0.4098	0.2016	0.0000	11.9117
HOS Ent_2^{17}	0.4998	0.2520	0.3407	0.1819	0.2281	0.1832	0.0000	11.3593
HOS EntPh^{1}	0.7459	0.1998	0.6556	0.2432	0.4517	0.2683	0.0001	10.2516
HOS EntPh^{2}	0.7362	0.1956	0.6320	0.2392	0.4473	0.1948	0.0001	9.9853
HOS Ent_3^{18}	0.3771	0.2831	0.2760	0.2464	0.0917	0.0809	0.0001	9.3878
HOS Ent_3^{17}	0.3733	0.2730	0.2200	0.1940	0.1329	0.1491	0.0004	8.1473
HOS EntPh^{3}	0.6822	0.1712	0.6131	0.2386	0.4362	0.2819	0.0006	7.7068
HOS Ent_2^{15}	0.4217	0.2517	0.2927	0.2058	0.1865	0.0848	0.0007	7.4890
Max Entropy	0.5113	0.1290	0.4551	0.1802	0.3361	0.1055	0.0009	7.1760
Shannon Entropy	0.5114	0.1290	0.4552	0.1802	0.3362	0.1055	0.0009	7.1668
HOS Ent_1^{13}	0.6304	0.1905	0.4513	0.1932	0.4239	0.2853	0.0012	6.9091
HOS EntPh^{5}	0.5973	0.2467	0.5969	0.2643	0.3995	0.2522	0.0012	6.8902
HOS Ent_1^{14}	0.5738	0.1570	0.4566	0.1958	0.3571	0.1954	0.0013	6.8567
HOS EntPh^{18}	0.7181	0.1473	0.6617	0.2037	0.5137	0.3012	0.0013	6.8303
HOS Ent_2^{5}	0.4406	0.1777	0.2723	0.1938	0.2760	0.1412	0.0015	6.6791
HOS Ent_3^{15}	0.3455	0.2917	0.2076	0.2326	0.0962	0.0639	0.0016	6.6110
HOS Ent_1^{8}	0.5020	0.2515	0.3873	0.2031	0.2887	0.1634	0.0027	6.0398
HOS Ent_1^{15}	0.4369	0.2022	0.3436	0.2007	0.2391	0.1042	0.0029	5.9725
Vajda Entropy	0.5855	0.1008	0.5309	0.1664	0.4316	0.1524	0.0031	5.9175
HOS EntPh^{4}	0.6561	0.2205	0.5962	0.2430	0.4387	0.2625	0.0032	5.8729
HOS EntPh^{13}	0.5743	0.2220	0.6546	0.2106	0.5142	0.2785	0.0038	5.6950
HOS Ent_3^{8}	0.3145	0.2908	0.1860	0.2051	0.1101	0.1091	0.0050	5.4098
HOS Ent_1^{7}	0.5670	0.2097	0.4393	0.1920	0.3743	0.2122	0.0054	5.3296
Rényi Entropy	0.3570	0.1494	0.3195	0.1986	0.2046	0.0653	0.0064	5.1556
HOS Ent_3^{5}	0.3035	0.2206	0.1632	0.1820	0.1597	0.1190	0.0064	5.1535
HOS EntPh^{11}	0.5673	0.2451	0.6571	0.2346	0.5168	0.2837	0.0081	4.9008
HOS Ent_1^{5}	0.5142	0.1342	0.3743	0.1950	0.4122	0.1566	0.0085	4.8580
HOS Ent_2^{8}	0.4130	0.2699	0.2931	0.2041	0.2218	0.1327	0.0090	4.7917
HOS EntPh^{6}	0.5586	0.2832	0.6034	0.2395	0.4574	0.2036	0.0108	4.6043
HOS Ent_3^{4}	0.2632	0.2400	0.1464	0.1526	0.1877	0.2312	0.0127	4.4388
HOS Ent_2^{16}	0.4236	0.2813	0.3011	0.2268	0.2231	0.1542	0.0146	4.2985
HOS Ent_2^{14}	0.4352	0.2624	0.3182	0.2009	0.2539	0.1989	0.0153	4.2494
HOS Ent_2^{7}	0.4643	0.2782	0.3282	0.2171	0.2768	0.2108	0.0176	4.1048
HOS Ent_3^{16}	0.3037	0.3070	0.1849	0.2145	0.1179	0.1160	0.0180	4.0802
HOS EntPh^{12}	0.6605	0.2570	0.6482	0.2303	0.5077	0.3412	0.0183	4.0613
HOS Ent_1^{2}	0.4787	0.1081	0.4183	0.1440	0.4904	0.1934	0.0207	3.9357
HOS Ent_2^{4}	0.4083	0.2592	0.2733	0.1858	0.3002	0.2590	0.0215	3.8967
HOS Ent_3^{14}	0.3149	0.2868	0.1977	0.1833	0.1618	0.1896	0.0248	3.7503
HOS Ent_2^{13}	0.4686	0.1793	0.3282	0.2145	0.3111	0.2859	0.0297	3.5640
HOS Ent_1^{11}	0.5281	0.1659	0.4365	0.1823	0.3801	0.2264	0.0342	3.4201
HOS Ent_1^{6}	0.5861	0.1697	0.4377	0.2403	0.4263	0.2389	0.0351	3.3931
HOS EntPh^{15}	0.6780	0.2541	0.6588	0.2414	0.5333	0.2839	0.0397	3.2655
HOS Ent_1^{10}	0.5380	0.1472	0.4720	0.1704	0.4083	0.1984	0.0440	3.1600

++HOS: higher order spectra; Ent: bispectrum entropy; EntPh: bispectrum phase entropy; the number in subscript corresponds to the order of the bispectrum entropy (i.e., first, second, or third); the number in superscript corresponds to the considered Radon angle.

36 listed in Table 2), with an accuracy of 97.6%, a PPV equal to 100%, a sensitivity equal to 96.4%, and a specificity equal to 100%.

Our results demonstrate indicate that, or system is able to correctly identify mild stroke in 100% of cases, and misdiagnosed a medium or severe stroke as mild in only 2.4% of cases (16 false negatives).

4. Discussion

It can be seen from the Table 2 that, most of the entropy features gradually decreases from LACS to PACS to TACS. The entropy values decreases depending on the severity of the brain stroke. In LACS, the change in the pixel value is very subtle, so the entropy values are large. In PACS and TACS, there will be more white patches resulting in the reduction of variability in the pixel values and entropy values.

Medical imaging technology is progressing toward higher resolution systems, and is capturing more images per patient (Ng, Faust, Sudarshan, & Chattopadhyay, 2015). For example, the field strength in MRI systems is increased to have higher signal-to-noise ratio with a better resolution which is suitable for clinical applications (Stucht

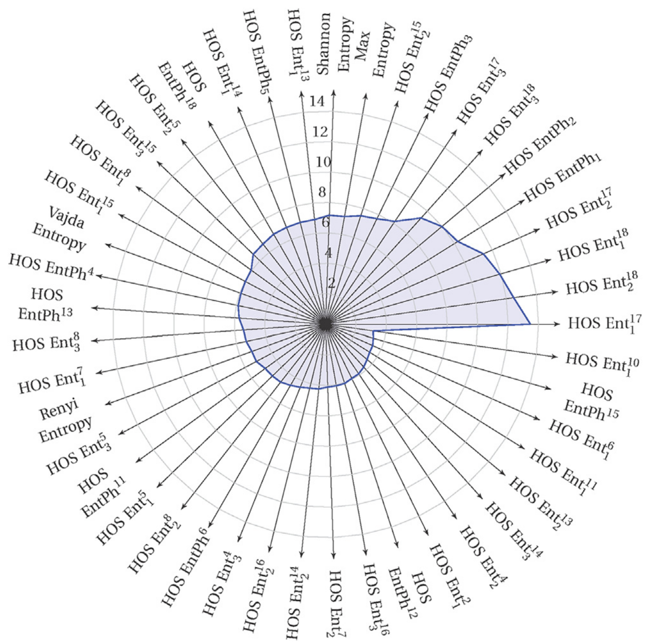

Fig. 4. Spider diagram to display the F-value for the individual features.

et al., 2015). That means that human interaction with these images becomes more labor intensive, since the cognitive processes involved in understanding images with more detail requires more time. That extended time requirement is amplified by the fact that there are more images available for analysis. Hence, the goal of decision support systems for reading cardiologists must be to reduce human interaction as much as possible. Ideally, a human decision maker should only be presented with suspected positive cases. In our case, the reading radiographer should only see the MRI images that show signs of the selected stroke severity. As a consequence, the automated stroke severity detection systems must have a high sensitivity to reduce the changes of missing true positives, i.e. MRI images showing the signs of the selected stroke severity. State-of-the art decision support systems do not meet these requirements. All of the support systems, as summarized in Table 4, utilize image segmentation techniques that require manual intervention. To be specific, the reading radiographer needs to determine, or at least to confirm, a region of interest within the MRI image. This is undesirable, because of the time

Table 3
Classification results for ischemic stroke identification.

Classifier	No. features	TP	TN	FP	FN	Acc. (%)	PPV (%)	Sens. (%)	Spec. (%)
DT	11	375	199	24	69	86.06	93.98	84.46	89.24
LDA	26	305	163	60	139	70.16	83.56	68.69	73.09
QDA	24	348	185	38	96	79.91	90.16	78.38	82.96
SVM Poly 1	45	329	221	2	115	82.46	99.40	74.10	99.10
SVM Poly 2	19	370	223	0	74	88.91	100.00	83.33	100.00
SVM Poly 3	10	359	222	1	85	87.11	99.72	80.86	99.55
k-NN	11	335	223	0	109	83.66	100.00	75.45	100.00
PNN	2	301	171	52	143	70.76	85.27	67.79	76.68
SVM RBF	36	428	223	0	16	97.60	100.00	96.40	100.00

++ TP: true positives; TN: true negatives; FP: false positives; FN: false negatives; Acc: accuracy; PPV: positive predictive value; Sens: sensitivity; Spec: specificity.

Table 4
Comparison with rest of the similar works.

Authors	Technique	Data	Performance
Mitra et al. (2014)	Bayesian-Markov Random Field	36 patients 3 month after stroke	Sensitivity of segmentation: 0.53 ± 0.13
Tsai et al. (2014)	Thresholding	22 patients with acute cerebral infarction	Similarity index $89.9 \pm 6.5\%$
Maier et al. (2015)	Clustering (Fuzzy)	37 patients	prec . = 0.80 and recall = 0.54 on average
Muda, Saad, Bakar, Muda, and Abdullah (2015)	Clustering (Fuzzy)	20 MRI images	Dice index 0.74
Griffis, Allendorfer, and Szaflarski (2016)	Image algebra	30 patients with left-hemisphere stroke of at least 6 months duration	Dice index 0.66
Chen, Bentley, and Rueckert (2017)	Deep learning	741 acute stroke patients	Lesion detection rate = 0.94.
Subudhi et al. (2018)	17 statistical and geometrical features	142 S patients	Accuracy of 85%
Subudhi et al. (2018)	Delaunay triangulation and texture features	192 MR brain images of stroke lesion	Sensitivity of 0.93, accuracy of 0.95
This study	HOS features	267 MRI images	Sensitivity = 96.4%, specificity = 100%, accuracy 97.6%, positive predictive value = 100%

required to identify the region of interest, and the training required to interact with the decision support system in an optimal way. Furthermore, indicating the region of interest is inevitably associated with problems of inter- and intra-observer variability, which limit diagnostic quality in a practical setting. In the current study, we have undertaken a different approach by using HOS features. Extracting these features does not require manual intervention; hence we established a truly automatic stroke severity evaluation.

The number of available datasets is crucial for the design of decision support systems, because that dataset limits the amount of transferrable knowledge concerning the disease that can be extracted. In our case, we require the decision support system to function in a practical environment, where all of the data is unknown, and the stroke severity must be estimated. That estimation is based upon the knowledge extracted from the dataset that was available during the design time. We have used 267 MRI images. These are increased from the number of images N used in prior work (Subudhi, Jena, & Sabut, 2018; Subudhi, Acharya, Dash, Jena, & Sabut, 2018). Hence, there is the possibility that our system may have improved performance in a practical setting.

The practical performance of a system cannot be established during design time. It is only possible to reason about the practical performance based upon statistical measures, such as the accuracy, sensitivity, and specificity. In our study, these measures were established with ten-fold cross validation, which provides a better estimate of the performance achievable for the available dataset. However, we did not attempt a blindfold validation of the system. Neither did any of the studies summarized in Table 4 implement a blindfold procedure. This is a shortcoming, because a blindfold validation mimics the use case scenario for the decision support system. The blindfold cases can be established by excluding specific patients from the dataset used for training and testing the classification system. The images from these patients are tested in a separate blindfold validation step. During the design time, we decided against blindfold validation, because it would have restricted the number of available datasets, and hence it would have limited the volume of extractable diagnostic knowledge.

5. Conclusion

In this paper, higher order spectra bispectrum entropy and phase features were used to extract salient information from MRI imagery, for stroke severity estimation. To establish a result, we built an automated decision support system which classifies MRI images as showing signs of PACS LACS or TACS. Through competitive testing, we established that the SVM RBF classifier outperformed DT, LDA, QDA, SVM Poly 1, SVM Poly 2, SVM Poly 3, k-NN and PNN. To be specific, the SVM RBF classifier achieved a sensitivity = 96.4%, specificity = 100%, accuracy 97.6%, and positive predictive value = 100%.

Our decision support system does not require any manual intervention from the reading radiographer. Hence, our method is automatic and not affected by inter- and intra-observer variability. We achieved this property by replacing features based on image segmentation results with higher order spectra bispectrum entropy and phase features. Despite that restriction, we were able to achieve a best classification performance among all of the surveyed studies.

We have achieved the specificity is 100%. This means that, our proposed system is able to automatically identify all the LACS images correctly. Hence, we will be able to identify the early stage of the brain stroke correctly.

Having a truly automatic stroke severity classification support system has the potential to reduce time and effort spent on routine cases. The reading radiographer can therefore focus on corner cases which require more manual effort to establish an accurate diagnosis.

Declaration of Competing Interest

The authors declared no conflict of interest in this work.

Appendix A. Supplementary material

Supplementary data to this article can be found online at https://doi.org/10.1016/j.cogsys.2019.05.005.

References

Acharya, U. R. et al. (2016). Automated characterization of fatty liver disease and cirrhosis using curvelet transform and entropy features extracted from ultrasound images. *Computers in Biology and Medicine, 79*(June), 250–258.

Acharya, U. R., Faust, O., Molinari, F., Sree, S. V., Junnarkar, S. P., & Sudarshan, V. (2015). Ultrasound-based tissue characterization and classification of fatty liver disease: A screening and diagnostic paradigm. *Knowledge-Based Systems, 75*, 66–77.

Bonita, R. (1992). Epidemiology of stroke. *Lancet (London, England), 339* (8789), 342–344.

Carson, C., Belongie, S., Greenspan, H., & Malik, J. (2002). Blobworld: Image segmentation using expectation-maximization and its application to image querying. *IEEE Transactions on Pattern Analysis and Machine Intelligence, 24*(8), 1026–1038.

Chen, L., Bentley, P., & Rueckert, D. (2017). Fully automatic acute ischemic lesion segmentation in DWI using convolutional neural networks. *NeuroImage: Clinical, 15*, 633–643.

Chin, C. L., Lin, B. J., Wu, G. R., Weng, T. C., Yang, C. S., Su, R. C., et al. (2017). An automated early ischemic stroke detection system using CNN deep learning algorithm. In Proceedings - 2017 IEEE 8th international conference on awareness science and technology, ICAST 2017, pp. 368–372. doi:10.1109/ICAwST.2017.8256481.

Chua, K. C., Chandran, V., Acharya, U. R., & Lim, C. M. (2008). Cardiac state diagnosis using higher order spectra of heart rate variability. *Journal of Medical Engineering & Technology, 32*(2), 145–155.

Chua, K. C., Chandran, V., Acharya, R., & Lim, C. M. (2008). Automatic identification of epilepsy by HOS and power spectrum parameters using EEG signals: A comparative study. In 2008 30th annual international conference of the IEEE engineering in medicine and biology society, pp. 3824–3827.

Duda, R., Hart, P., & Stork, D. (2012). *Pattern Classification.*

Feng, C., Zhao, D., & Huang, M. (2016). *Segmentation of ischemic stroke lesions in multi-spectral MR images using weighting suppressed FCM and three phase level set*. Cham: Springer (pp. 233–245).

Griffis, J. C., Allendorfer, J. B., & Szaflarski, J. P. (2016). Voxel-based Gaussian naïve Bayes classification of ischemic stroke lesions in individual T1-weighted MRI scans. *Journal of Neuroscience Methods, 257*, 97–108.

He Haibo, Bai Yang, Garcia E. A., & Li Shutao (2008) ADASYN: Adaptive synthetic sampling approach for imbalanced learning. In 2008 IEEE international joint conference on neural networks (IEEE world congress on computational intelligence), pp. 1322–1328.

Hemanth, D. J., Vijila, C. K. S., Selvakumar, A. I., & Anitha, J. (2013). Distance metric-based time-efficient fuzzy algorithm for abnormal magnetic resonance brain image segmentation. *Neural Computing and Applications, 22*(5), 1013–1022.

Hevia-Montiel, N. et al. (2007) Robust nonparametric segmentation of infarct lesion from diffusion-weighted MR images. In 2007 29th annual international conference of the IEEE engineering in medicine and biology society, pp. 2102–2105.

Hoaglin, D. C., & Welsch, R. E. (1978). The hat matrix in regression and ANOVA. *American Statistician, 32*(1), 17–22.

Ji, Z., Xia, Y., & Zheng, Y. (Nov. 2017). Robust generative asymmetric GMM for brain MR image segmentation. *Computer Methods and Programs in Biomedicine, 151*, 123–138.

Lindgren, A., Norrving, B., Rudling, O., & Johansson, B. B. (1994). Comparison of clinical and neuroradiological findings in first-ever stroke. A population-based study. *Stroke, 25*(7), 1371–1377.

Lutsep, H. L., Albers, G. W., Decrespigny, A., Kamat, G. N., Marks, M. P., & Moseley, M. E. (1997). Clinical utility of diffusion-weighted magnetic resonance imaging in the assessment of ischemic stroke. *Annals of Neurology, 41*(5), 574–580.

Maier, O., Wilms, M., von der Gablentz, J., Krämer, U. M., Münte, T. F., & Handels, H. (2015). Extra tree forests for sub-acute ischemic stroke lesion segmentation in MR sequences. *Journal of Neuroscience Methods, 240*, 89–100.

Martis, R. J., Acharya, U. R., Mandana, K. M., Ray, A. K., & Chakraborty, C. (2013). Cardiac decision making using higher order spectra. *Biomedical Signal Processing and Control, 8*(2), 193–203.

Mitra, J. et al. (2014). Lesion segmentation from multimodal MRI using random forest following ischemic stroke. *Neuroimage, 98*, 324–335.

Mitra, J., Bourgeat, P., Fripp, J., Ghose, S., Rose, S., Salvado, O., et al. (2014). Lesion segmentation from multimodal MRI using random forest following ischemic stroke. *NeuroImage, 98*, 324–335.

Molinari, F., Raghavendra, U., Gudigar, A., Meiburger, K. M., & Rajendra Acharya, U. (2018). An efficient data mining framework for the characterization of symptomatic and asymptomatic carotid plaque using bidimensional empirical mode decomposition technique. *Medical and Biological Engineering and Computing*.

Muda, A. F., Saad, N. M., Bakar, S. A. A., Muda, S., & Abdullah, A. R. (2015). Brain lesion segmentation using fuzzy C-means on diffusion-weighted imaging. *ARPN Journal of Engineering and Applied Sciences, 10*(3), 1138–1144.

Newcombe, V. F. J., Das, T., & Cross, J. J. (2013). Diffusion imaging in neurological disease. *Journal of Neurology, 260*(1), 335–342.

Ng, K. H., Faust, O., Sudarshan, V., & Chattopadhyay, S. (2015). Data overloading in medical imaging: Emerging issues, challenges and opportunities in efficient data management. *Journal of medical imaging and health informatics, 5*(4), 755–764.

Nikias, C. L., & Raghuveer, M. R. (1987). Bispectrum estimation: A digital signal processing framework. *Proceedings of the IEEE, 75*(7), 869–891.

Noronha, K. P., Acharya, U. R., Nayak, K. P., Martis, R. J., & Bhandary, S. V. (2014). Automated classification of glaucoma stages using higher order cumulant features. *Biomedical Signal Processing and Control, 10*(1), 174–183.

Osmani, A. H., Durrani, R. K., & Ara, J. (2010). Comparison of outcome in different types of stroke due to cerebral ischemia. *Journal of the College of Physicians and Surgeons Pakistan, 20*(1), 42–46.

Pizer, S. M. et al. (1987). Adaptive histogram equalization and its variations. *Computer Vision, Graphics Image Processing, 39*(3), 355–368.

Radon, J. (1986). On the determination of functions from their integral values along certain manifolds. *IEEE Transactions on Medical Imaging, 5*(4), 170–176.

Raghavendra, U. et al. (2018). Optimized multi-level elongated quinary patterns for the assessment of thyroid nodules in ultrasound images. *Computers in Biology and Medicine, 95*.

Ramli, D. A., Ghazali, N., & Tay, L. (2018). Ischemic stroke detection system with computer aided diagnostic capability. *Procedia Computer Science, 126*, 393–402. https://doi.org/10.1016/j.procS.2018.07.273.

Scalzoa, D. S. L., Fabien, Jeffry R., Alger, Xiao Hu, Saver, Jeffrey L., Dani, Krishna A., Muirc, Keith W., ... Warach, Steven (2013). Multi-center prediction of hemorrhagic transformation in acute ischemic stroke using permeability imaging features. *Magnetic Resonance Imaging, 31*(6), 961–969.

Singh, A. P., & Singh, B. (2010). *Texture features extraction in mammograms using non-Shannon entropies*. Dordrecht: Springer (pp. 341–351).

Sridevi, M., & Mala, C. (2019). Self-organizing neural networks for image segmentation based on multiphase active contour. *Neural Computing and Application*, 1–12.

Stucht, D., Danishad, K. A., Schulze, P., Godenschweger, F., Zaitsev, M., & Speck, O. (2015). Highest resolution in vivo human brain MRI using prospective motion correction. *PloS One, 10*(7), p.e0133921.

Subudhi, A., Acharya, U. R., Dash, M., Jena, S., & Sabut, S. (2018). Automated approach for detection of ischemic stroke using Delaunay Triangulation in brain MRI images. *Computers in Biology and Medicine*.

Subudhi, A., Jena, S., & Sabut, S. (2018). Delineation of the ischemic stroke lesion based on watershed and relative fuzzy connectedness in brain MRI. *Medical & Biological Engineering & Computing, 56*(5), 795–807.

Subudhia, A., Dash, M., Jena, S., & Sabut, S. (2018). Automated approach for detection of ischemic stroke using Delaunay Triangulation in brain MRI images. *Computers in Biology and Medicine, vol*, in press.

Swapna, G., Rajendra Acharya, U., Vinithasree, S., & Suri, J. S. (2013). Automated detection of diabetes using higher order spectral features extracted from heart rate signals. *Intelligent Data Analysis, 17*(2), 309–326.

Tsai, J. Z., Peng, S. J., Chen, Y. W., Wang, K. W., Wu, H. K., Lin, Y. Y., ... Yeh, P. S. (2014). Automatic detection and quantification of acute cerebral infarct by fuzzy clustering and histographic characterization on diffusion weighted MR imaging and apparent diffusion coefficient map. *BioMed Research International*.

Wang, Y., Xiang, S., Pan, C., Wang, L., & Meng, G. (2013). Level set evolution with locally linear classification for image segmentation. *Pattern Recognition, 46*(6), 1734–1746.

Zaidi, S. F. et al. (2012). Final infarct volume is a stronger predictor of outcome than recanalization in patients with proximal middle cerebral artery occlusion treated with endovascular therapy. *Stroke, 43*(12), 3238–3244.

Please cite this article as: U. Rajendra Acharya, K. M. Meiburger, O. Faust et al., Automatic detection of ischemic stroke using higher order spectra features in brain MRI images , Cognitive Systems Research, https://doi.org/10.1016/j.cogsys.2019.05.005